

Polarized Charge Dynamics of a Novel Charge Density Wave in Kagome FeGe

Shaohui Yi,^{1,2,*} Zhiyu Liao,^{1,2,*} Qi Wang,^{3,4,*} Haiyang Ma,³ Jianpeng Liu,³ Xiaokun Teng,⁵ Pengcheng Dai,⁵ Yaomin Dai,⁶ Jianzhou Zhao,^{7,†} Yanpeng Qi,^{3,4,8,‡} Bing Xu,^{1,2,§} and Xianggang Qiu^{1,2,¶}

¹*Beijing National Laboratory for Condensed Matter Physics, Institute of Physics, Chinese Academy of Sciences, P.O. Box 603, Beijing 100190, China*

²*School of Physical Sciences, University of Chinese Academy of Sciences, Beijing 100049, China*

³*School of Physical Science and Technology, ShanghaiTech University, Shanghai 201210, China*

⁴*ShanghaiTech Laboratory for Topological Physics, ShanghaiTech University, Shanghai 201210, China*

⁵*Department of Physics and Astronomy, Rice University, Houston, Texas, USA*

⁶*National Laboratory of Solid State Microstructures and Department of Physics, Nanjing University, Nanjing 210093, China*

⁷*Co-Innovation Center for New Energetic Materials,*

Southwest University of Science and Technology, Mianyang 621010 Sichuan, China

⁸*Shanghai Key Laboratory of High-resolution Electron Microscopy, ShanghaiTech University, Shanghai 201210, China*

(Dated: March 18, 2024)

We report on the charge dynamics of kagome FeGe, an antiferromagnet with a charge density wave (CDW) transition at $T_{\text{CDW}} \simeq 105$ K, using polarized infrared spectroscopy and band structure calculations. We reveal a pronounced optical anisotropy, various excitations associated with flat bands and van Hove singularities (VHSs), and a moderate level of electronic correlations. Notably, there are two types of remarkable spectral weight (SW) redistributions for above and below T_{CDW} . The former involves a transfer between incoherent and coherent excitations driven by the magnetic splitting-induced elevation of flat bands. The latter manifests itself as a sudden change of SW from low to high energies for both a and c directions, suggesting a first-order transition and the three-dimensional nature of CDW. These anomalies in SW significantly differ from those observed in other kagome metals like CsV₃Sb₅, where the nesting of VHSs results in a pronounced CDW gap feature. Instead, our findings can be accounted for by the jump of VHSs relative to the Fermi energy via a first-order structural transition involving large partial Ge1-dimerization. Our study thus unveils a complex interplay among structure, magnetism, electronic correlations, and charge order in FeGe, offering valuable insights for a comprehensive understanding of CDW order in kagome systems.

The kagome lattice, a hexagonal network of corner-sharing triangles, has been studied for over 70 years [1]. Its unique band structure features the coexistence of flat bands (FBs), Dirac crossings, and van Hove singularities (VHSs), making it an excellent platform for studying the variety of emergent quantum phases resulting from the complex interplay between geometry, topology, and electronic correlations. In the early days, research mainly focused on the geometric spin frustration, showing its great potential to realize quantum spin liquid states [2–5]. Subsequently, a range of topological quantum states have been explored, such as Weyl fermions in Co₃Sn₂S₂ [6–8], Dirac fermions and flat bands in CoSn [9], and Chern gapped Dirac fermions in TbMn₆Sn₆ [10]. More recently, charge density wave (CDW) and unconventional superconductivity [11–14], as well as other exotic quantum phenomena, including electronic nematicity [15], roton pair density wave [16], and giant anomalous Hall effect [17], have been reported in the non-magnetic kagome metals AV₃Sb₅ ($A = \text{Cs, K, Rb}$).

Generally, the discovered kagome materials can only host either magnetism or charge orders, owing to the large energy separation between the FBs and the vHSs. However, lately, a CDW order ($T_{\text{CDW}} \simeq 100$ K) has been found inside the antiferromagnetic (AFM) phase of kagome FeGe ($T_N \simeq 410$ K) [18]. This CDW transition

is associated with an increase of ordered magnetic moments [19], which demonstrates an intertwined nature of magnetism and charge order (CO) in FeGe, thus offering a unique opportunity to explore a novel CDW with magnetism. Currently, the origin of CDW in FeGe is still full of controversy [18–32]. The nesting of VHSs at the M point and electron-phonon coupling were initially proposed to explain the formation of CDW [18–20], similar to AV₃Sb₅ [33–41]. However, Wu *et al.* found that the maximum nesting function of FeGe is at the K point instead of the M point, and suggested the key role of electronic correlations for CDW [21]. Additionally, electronic correlations induces a softening effect along the L-H direction in the calculated phonon spectrum of FeGe [29–31]. Furthermore, recent theoretical calculations and angle-resolved photoemission spectroscopy (ARPES) measurements in annealed samples support a new mechanism, in which the large dimerization partial Ge1-dimerization reduces the magnetic energy and leads to a stable $2 \times 2 \times 2$ CDW ground state [22, 23], in sharp contrast to AV₃Sb₅. Therefore, to clarify the origin of CDW in FeGe, a systematic study of charge dynamics across various electronic states or phases is essential.

In this letter, we utilize polarized optical spectroscopy and density functional theory (DFT) calculations to systematically study the charge dynamics of FeGe spanning

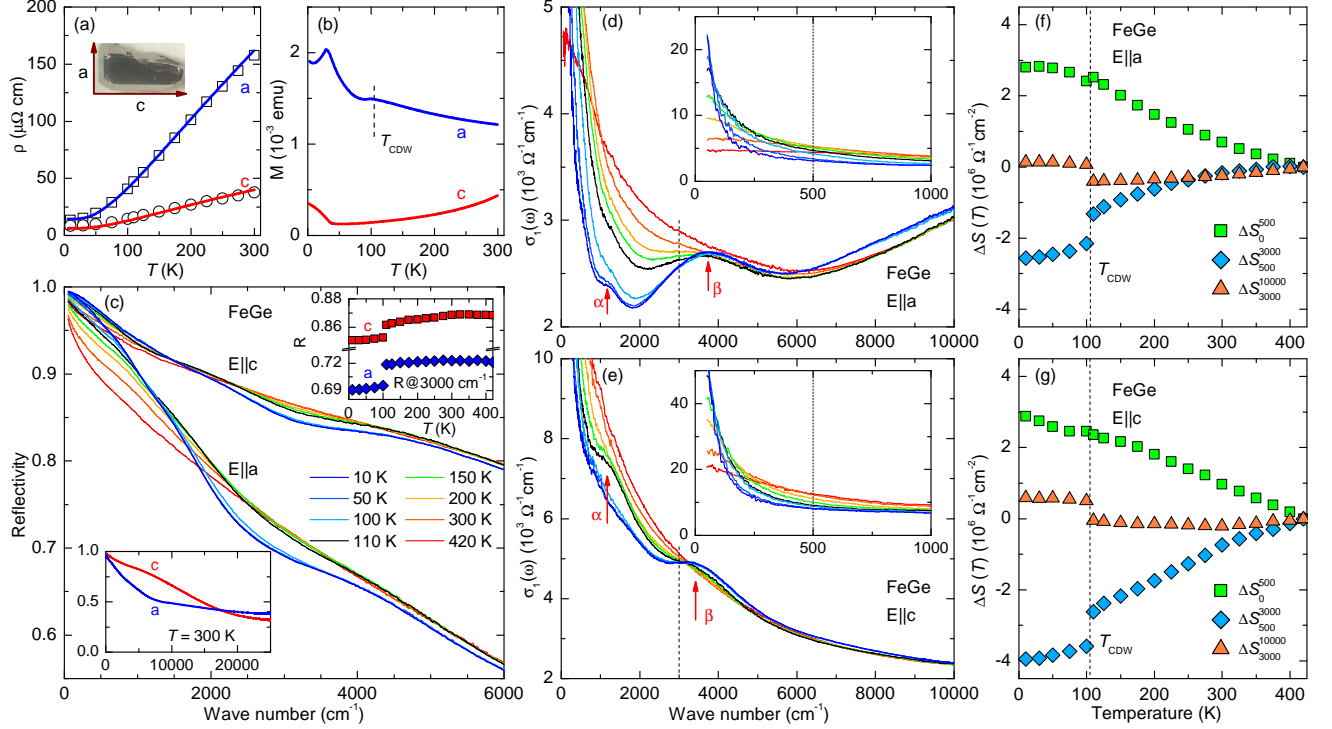


Figure 1. (color online) (a) Temperature dependence of resistivity along the a -axis and c -axis for kagome FeGe. The open symbols represent $\rho \equiv 1/\sigma_1(\omega \rightarrow 0)$ obtained by the Drude fits to the optical data. (b) Temperature dependence of the magnetization curves $M_a(T)$ and $M_c(T)$ measured at a 1 T magnetic field. (c) Temperature-dependent spectra of reflectivity $R(\omega)$ for $\mathbf{E} \parallel a$ and $\mathbf{E} \parallel c$. Bottom inset: Spectra up to 25 000 cm^{-1} at 300 K. Top inset: Temperature dependence of $R(\omega = 3000 \text{ cm}^{-1})$. (d) and (e) Temperature-dependent spectra of optical conductivity $\sigma_1(\omega)$ for $\mathbf{E} \parallel a$ and $\mathbf{E} \parallel c$, respectively. Insets provide the enlarged view of $\sigma_1(\omega)$ in the far-infrared region. (f) and (g) The corresponding changes of the spectral weight, $\Delta S(T) = S(T) - S(420\text{K})$, for $\mathbf{E} \parallel a$ and $\mathbf{E} \parallel c$, respectively.

from paramagnetic (PM) to AFM and to CDW phases. Our study reveals significant optical anisotropy and a variety of intraband and interband excitations associated with VHSs and FBs. Particularly noteworthy is the magnetization-induced shift of FBs and the CDW transition, which result in two distinct types of spectral weight (SW) redistributions. Furthermore, we observe that the CDW response lacks a gap feature and exhibits characteristics of a first-order transition, contrasting with observations in AV_3Sb_5 . Our results thus are consistent with the novel CDW mechanism based on a first-order structural transition involving large partial Ge1-dimerization.

Sample synthesis, experimental methods, and details of Drude-Lorentz analysis and DFT calculations are provided in the Supplemental Material.

Figure 1(a) displays the temperature (T) dependence of the resistivity for kagome FeGe along the a -axis and c -axis. Both directions exhibit typical metallic behavior and manifest strong electronic anisotropy with lower resistivity along the c -axis. In Fig. 1(b), the T -dependent magnetizations, $M_a(T)$ and $M_c(T)$, show notable magnetic anisotropy. Upon cooling, $M_a(T)$ gradually increases and shows an anomaly at the CDW transition ($T_{\text{CDW}} \simeq 105 \text{ K}$). In contrast, $M_c(T)$ decreases and then

turns upward below $T_{\text{Cant}} \simeq 60 \text{ K}$, attributed to spin canting. These observations are consistent with previous studies [18].

Due to the electronic and magnetic anisotropies, we measured the polarized reflectivity $R(\omega)$ of FeGe. In Fig. 1(c), $R(\omega)$ is presented up to 6000 cm^{-1} from 420 to 10 K for $\mathbf{E} \parallel a$ and $\mathbf{E} \parallel c$. The bottom inset compares $R_a(\omega)$ and $R_c(\omega)$ at $T = 300 \text{ K}$ up to 25 000 cm^{-1} . In the infrared region, $R_c(\omega)$ is much higher than $R_a(\omega)$, indicating an optical anisotropy consistent with the lower resistivity along the c -axis. In the low-frequency limit, both $R_a(\omega)$ and $R_c(\omega)$ approach unity and increase with decreasing T , reflecting the metallic nature of FeGe. Furthermore, there is no clear anomalous change across the AFM transition ($T_{\text{N}} \simeq 410 \text{ K}$) for both polarizations. However, below T_{CDW} , $R(\omega)$ shows a sudden drop in the range of 2000 – 5000 cm^{-1} . Such a sudden change, as highlighted by the T -evolution of $R(\omega = 3000 \text{ cm}^{-1})$ in the top inset, provides an initial spectroscopic indication of a first-order CDW transition in FeGe, which is consistent with the neutron [18], x-ray scattering [29], and Raman experiments [24].

The optical conductivity $\sigma_1(\omega)$ provides direct information about the charge dynamics. Fig. 1(d) and

Fig. 1(e) display the T -dependent $\sigma_{1a}(\omega)$ and $\sigma_{1c}(\omega)$ for $\mathbf{E} \parallel a$ and $\mathbf{E} \parallel c$, respectively. In the far-infrared region, $\sigma_1(\omega)$ is dominated by a Drude-like peak, and $\sigma_{1c}(\omega)$ is about twice higher than $\sigma_{1a}(\omega)$, indicating a strong three-dimensional (3D) metallic response. With decreasing T , the Drude peak narrows and exhibits coherent behavior at low temperatures, as emphasized in the insets. In the mid-infrared region ($500 - 3000 \text{ cm}^{-1}$), $\sigma_1(\omega)$ decreases and transfers the SW to lower frequencies. Meanwhile, an absorption peak (labeled as β) gradually appears around 4000 cm^{-1} . Across the CDW transition, $\sigma_1(\omega)$ below 3000 cm^{-1} is further suppressed, while its associated SW is transferred to the β peak and other high-energy interband transitions. Both $\sigma_{1a}(\omega)$ and $\sigma_{1c}(\omega)$ exhibit similar features, particularly in their responses to the CDW transition, providing strong evidence for the formation of a 3D CDW state in FeGe, consistent with the $2 \times 2 \times 2$ CDW order observed from other experiments [25, 26]. Additionally, with the narrowing of the Drude peak or the CDW transition, a low-energy peak (labeled as α) emerges around 1200 cm^{-1} .

The T -dependent spectral changes have been further analyzed in terms of the partial SW, $S_{\omega_a}^{\omega_b}(T) = \int_{\omega_a}^{\omega_b} \sigma_1(\omega, T) d\omega$, restricted by the cutoff frequencies ω_a and ω_b . This approach allows us to specify the SW changes of different electronic excitations by choosing suitable ω_a and ω_b . Fig. 1(f) and Fig. 1(g) detail the SW changes, $\Delta S(T) = S(T) - S(420 \text{ K})$, at various restricted frequency ranges for $\mathbf{E} \parallel a$ and $\mathbf{E} \parallel c$, respectively. For ΔS_0^{500} and ΔS_{500}^{3000} , that are governed by the coherent and incoherent excitations, respectively, the transfer of incoherent to coherent excitations leads to an increase in ΔS_0^{500} and a corresponding decrease in ΔS_{500}^{3000} at $T > T_{\text{CDW}}$. For ΔS_{3000}^{10000} , dominated by the β peak and other high-energy excitations, it remains nearly T -independent. As $T < T_{\text{CDW}}$, ΔS_0^{500} undergoes a slight suppression and ΔS_{500}^{3000} is suddenly reduced, while ΔS_{3000}^{10000} is enhanced, indicating an abrupt SW transfer from low to high frequencies due to the CDW transition. Additionally, ΔS_{500}^{3000} and ΔS_{3000}^{10000} exhibit more significant anomalies compared to ΔS_0^{500} , implying a more pronounced impact of CDW on incoherent excitations than on coherent ones.

To perform a quantitative analysis of various intra- and interband excitations, we employed the Drude-Lorentz model to fit the measured $\sigma_1(\omega)$ spectra. Fig. 2(a) shows the decomposition of $\sigma_{1a}(\omega)$ at $T = 110 \text{ K}$. A similar decomposition of $\sigma_{1c}(\omega)$ is available in the Supplemental Materials. The fitting curve consists of two Drude terms (labeled as D1 and D2), along with three Lorentz terms (labeled as α , β , and γ) that account for interband transitions at higher energies. The two-Drude fit suggests two types of charge carriers with different scattering rates. Specifically, the scattering rate ($1/\tau$) of D1 is quite smaller compared to that of D2, e.g., $1/\tau_{D1} = 130 \text{ cm}^{-1}$ and $1/\tau_{D2} = 1000 \text{ cm}^{-1}$ at 110 K .

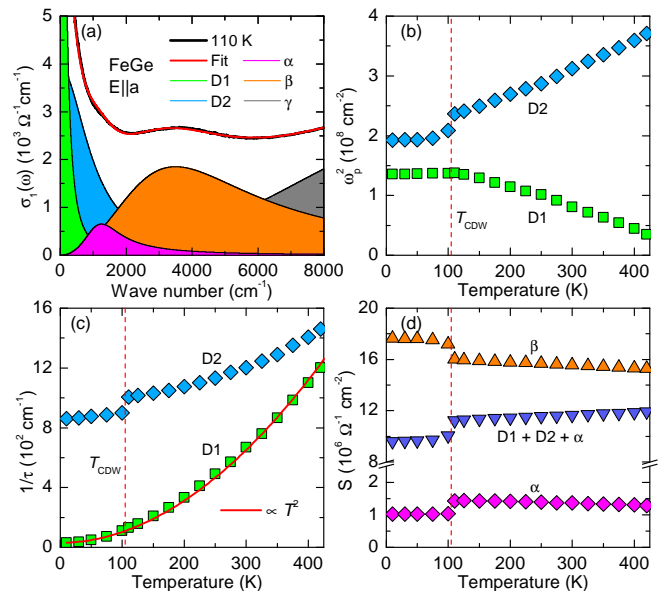


Figure 2. (color online) (a) Decomposition of $\sigma_1(\omega)$ spectra at $T = 110 \text{ K}$ for $\mathbf{E} \parallel a$ using a Drude-Lorentz model. (b) and (c) Temperature dependence of the Drude weights ω_p^2 and scattering rates $1/\tau$, respectively. (d) Temperature-dependent spectral weight of various individual and combined components.

The Drude fit also enables the extraction of the dc resistivity, $\rho \equiv 1/\sigma_1(\omega \rightarrow 0)$, as shown by open symbols in Fig. 1(a), which aligns well with the results from the dc transport measurement. With decreasing T , D1 exhibits a Fermi-liquid behavior with $1/\tau \propto T^2$ and a substantial increase in weight (proportional to ω_p^2), while D2 shows a slight decrease in $1/\tau$ and a corresponding loss in weight, as shown in Figs. 2(b-c). The compensated changes of weights for D1 and D2 imply a T -induced shift of bands near the Fermi energy (E_F). Notably, the CDW transition only has a strong impact on D2 (i.e., the incoherent excitations), where ω_p^2 and $1/\tau$ for D2 show an abrupt suppression at $T < T_{\text{CDW}}$, whereas those for D1 show no anomalies. In Fig. 2(d), we revealed a sudden decrease (increase) in the SW of the α (β) band at T_{CDW} . Overall, the CDW results in a sudden SW redistribution between the low-energy (two Drude and α bands) and high-energy components (β and other high-energy bands).

Next, to unravel the origin of each component in $\sigma_1(\omega)$, we calculated the band structure of FeGe in both the PM and AFM phases. In the PM phase, as shown in Fig. 3(a), the band structure features a pair of typical kagome bands along the Γ -M-K- Γ direction, where the FBs (marked by a grey bar) are situated around E_F , VHSs (VHS1 and VHS2) are below E_F at the M point and Dirac crossings are present at the K point. As shown in Fig. 3(b), the AFM order shifts the FBs upward above E_F and brings the VHSs closer to E_F , particularly for VSH1. Additionally, a highly dispersive band emerges

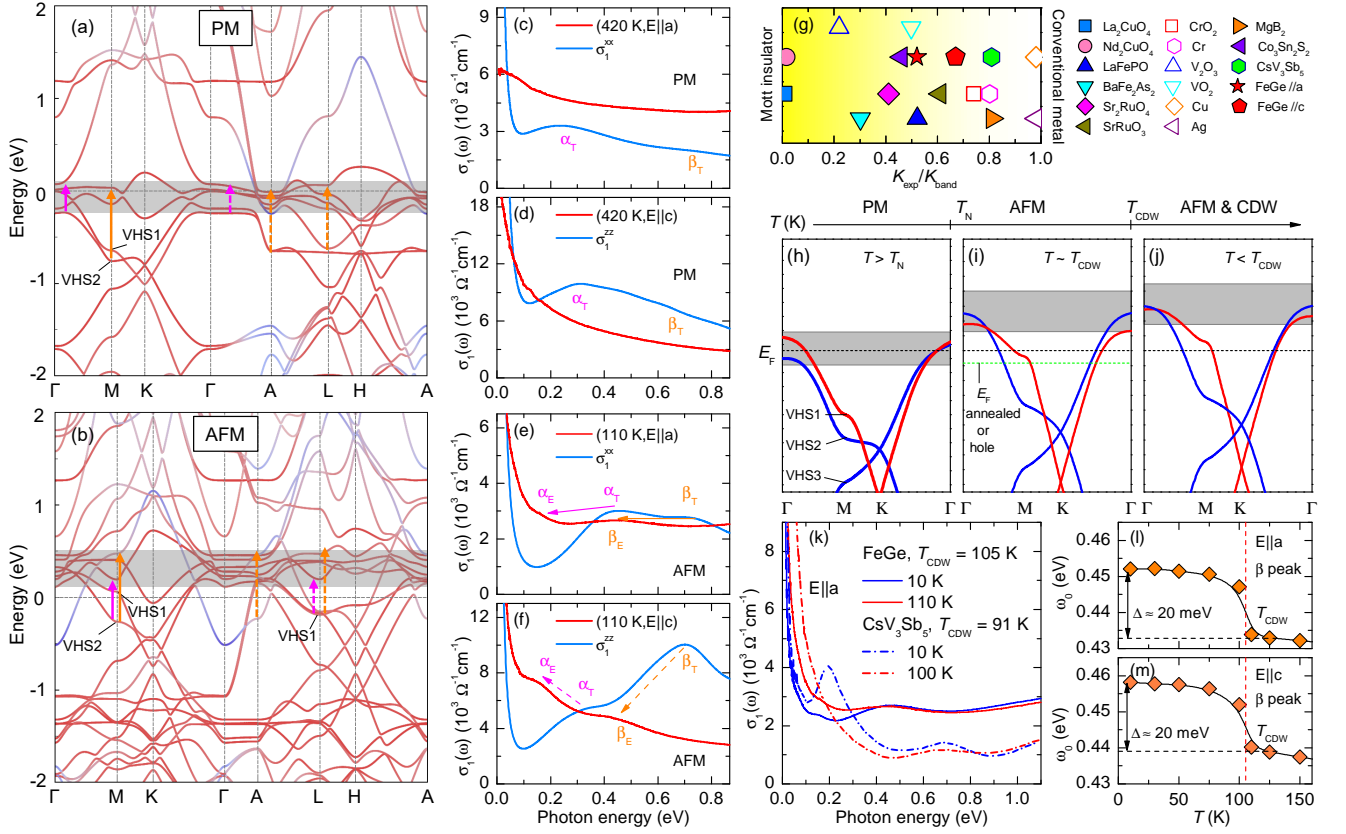


Figure 3. (color online) (a) and (b) Band structure of FeGe calculated in the PM and AFM phases, respectively. (c–f) Comparisons of the calculated and experimental $\sigma_1(\omega)$. (g) The ratio of kinetic energy $K_{\text{exp}}/K_{\text{band}}$ for FeGe. The values for other materials are obtained from Refs. [42, 43] and the references cited therein. (h–j) A simplified schematic summary of magnetization-induced changes of band structure. (k) Comparison of $\sigma_1(\omega)$ between FeGe and CsV_3Sb_5 . (l) and (m) show the jump of peak position of β band at the CDW transition for $\mathbf{E} \parallel a$ and $\mathbf{E} \parallel c$, respectively.

around the Γ point and intersects with E_F . In Figs. 3(c–f), we compared the calculated and experimental $\sigma_1(\omega)$ spectra. In the PM phase, the calculated $\sigma_1^{xx}(\omega)$ displays three features: a Drude response of intraband transitions of FBs, an α peak of interband transitions between the bottom and top FBs at ~ 0.25 eV (magenta arrows), and a β peak of interband transitions between VHSs and top FBs at ~ 0.75 eV (orange arrows). The $\sigma_1^{zz}(\omega)$ exhibits similar features, but with almost twice the strength of the response. In the experimental $\sigma_1(\omega)$ spectra above T_N , these features are smeared out due to the strong thermal broadening effect at $T = 420$ K. In the AFM phase, the calculated α_T peak loses SW, while the β_T peak gains SW, due to all FBs are elevated above E_F , resulting in the α peak being replaced by the interband transitions between VHSs and the bottom FBs. Compared to theoretical results, the experimental α_E and β_E peaks shift significantly to lower energies, with $\omega_0^\alpha = 0.43 \rightarrow 0.17$ eV and $\omega_0^\beta = 0.75 \rightarrow 0.45$ eV for $\mathbf{E} \parallel a$, and $\omega_0^\alpha = 0.32 \rightarrow 0.17$ eV and $\omega_0^\beta = 0.70 \rightarrow 0.46$ eV for $\mathbf{E} \parallel c$.

The significant position shift of interband transitions between the experimental and theoretical results suggests

a strong renormalization of band structure caused by electronic correlations. Since the β peak is mainly dominated by the interband transitions within the kagome bands (i.e., between VHSs and FBs), the ratio $\omega_0^{\beta,T}/\omega_0^{\beta,E}$ can serve as a reliable estimation for the strength of electronic correlations. Here, $\omega_0^{\beta,T}/\omega_0^{\beta,E} = 1.67$ and 1.52 for $\mathbf{E} \parallel a$ and $\mathbf{E} \parallel c$, respectively, which agrees well with the renormalization factor of 1.6 observed in ARPES measurements [19] and dynamical mean-field theory calculations [29, 44]. Furthermore, the ratio of the experimental kinetic energy K_{exp} to that from band theory K_{band} also provides crucial information about electronic correlations, where K_{exp} or K_{band} is proportional to the SW of the Drude component. Fig. 3(g) summarizes $K_{\text{exp}}/K_{\text{band}}$ for FeGe and several other representative materials. Details about the determination of $K_{\text{exp}}/K_{\text{band}}$ are included in the Supplemental Materials. In FeGe, $K_{\text{exp}}/K_{\text{band}}$ is 0.52 ± 0.05 and 0.67 ± 0.05 for $\mathbf{E} \parallel a$ and $\mathbf{E} \parallel c$, respectively, suggesting a moderate strength of electronic correlations, which falls between $\text{Co}_3\text{Sn}_2\text{S}_2$ and CsV_3Sb_5 .

Electronic correlations and, in particular, magnetism, have pronounced effects on the band structure in kagome

materials. For instance, in $\text{Co}_3\text{Sn}_2\text{S}_2$ the magnetic splitting of bands shifts the FBs and Weyl points toward E_F , making electrons possess the properties of both correlation and topology. Similarly, as summarized in Figs. 3(h)–(j), the magnetic splitting in FeGe, which is proportional to the ordered magnetic moment [19], elevates the VHSs close to E_F , improving the activity of electronic states and thus the possibility of CDW instability. However, unlike the nesting mechanism of VHSs in AV_3Sb_5 , our experimental observations suggest a different origin of CDW in FeGe. As compared in Fig. 3(k), CsV_3Sb_5 and FeGe exhibit distinct charge responses to the CDW transition. The former shows a clear gap feature of CDW due to the nesting of VHSs around the M-point [38], whereas these features are absent in the latter. Recent theoretical calculations and ARPES measurements in FeGe provide a novel CDW mechanism, where the CDW is primarily driven by saving magnetic energies via a first-order structural transition involving large partial Ge1-dimerization [22, 23]. ARPES experiments on annealed samples did not detect the CDW gap but instead a sudden jump of bands originating from the enhanced spin-polarization in the CDW phase [23]. Our findings of charge dynamics are fully consistent with these above theoretical and experimental facts, thus supporting such a novel CDW mechanism.

Accordingly, the sudden SW changes at the CDW transition can be explained by the jump of VHS1 relative to E_F . Specifically, as illustrated in Figs. 3(i–j), VHS1 lies slightly below E_F at $T \sim T_{\text{CDW}}$ and then abruptly shifts above E_F at $T < T_{\text{CDW}}$ for our sample. This band jump is also evident in the shift of the β peak. As demonstrated in the Figs. 3(l–m), the β peak shows an increase of about 20 meV after the CDW transition, which is consistent with the results of the ARPES experiments [23]. Note that, in annealed or hole-doped samples, since VHS1 is already positioned above E_F at $T \sim T_{\text{CDW}}$ (marked by green dashed line) due to stronger magnetic moment [23, 45] or hole doping, the further upward shift of VHS1 at $T < T_{\text{CDW}}$ may not result in obvious changes in SW. This may clarify why another recent optical study on FeGe did not find strong SW redistributions under the CDW transition [46].

In summary, our optical conductivity measurements revealed rich information about the charge dynamics in FeGe, including a remarkable optical anisotropy, moderate electronic correlations, unconventional SW redistributions associated with magnetization-induced band shift and CDW transition, as well as a first-order transition and 3D character of CDW. These findings contrast with the conventional CDW mechanism observed in other kagome metals, and instead highlight a novel mechanism involving the intricate interplay among structure, magnetism, electronic correlations, and charge order in FeGe.

We acknowledge discussions with Yilin Wang and Kai Wang. This work was supported by the National Nat-

ural Science Foundation of China (Grant No. 12274442 and No. 52272265) and the National Key R&D Program of China (Grant No. 2022YFA1403901 and No. 2023YFA1607400).

* These authors contributed equally to this work.

† jzzhao@swust.edu.cn

‡ qiyp@shanghaitech.edu.cn

§ bingxu@iphy.ac.cn

¶ xgqiu@iphy.ac.cn

- [1] I. Syözi, Statistics of Kagomé Lattice, *Progress of Theoretical Physics* **6**, 306 (1951).
- [2] L. Balents, M. P. A. Fisher, and S. M. Girvin, Fractionalization in an easy-axis Kagome antiferromagnet, *Phys. Rev. B* **65**, 224412 (2002).
- [3] P. Anderson, Resonating valence bonds: A new kind of insulator?, *Materials Research Bulletin* **8**, 153 (1973).
- [4] L. Balents, Spin liquids in frustrated magnets, *Nature* **464**, 199 (2010).
- [5] S. Yan, D. A. Huse, and S. R. White, Spin-Liquid Ground State of the $S = 1/2$ Kagome Heisenberg Antiferromagnet, *Science* **332**, 1173 (2011).
- [6] E. Liu, Y. Sun, N. Kumar, L. Muechler, A. Sun, L. Jiao, S.-Y. Yang, D. Liu, A. Liang, Q. Xu, J. Kroder, V. Stüf, H. Borrmann, C. Shekhar, Z. Wang, C. Xi, W. Wang, W. Schnelle, S. Wirth, Y. Chen, S. T. B. Goennenwein, and C. Felser, Giant anomalous Hall effect in a ferromagnetic kagome-lattice semimetal, *Nature Physics* **14**, 1125 (2018).
- [7] D. F. Liu, A. J. Liang, E. K. Liu, Q. N. Xu, Y. W. Li, C. Chen, D. Pei, W. J. Shi, S. K. Mo, P. Dudin, T. Kim, C. Cacho, G. Li, Y. Sun, L. X. Yang, Z. K. Liu, S. S. P. Parkin, C. Felser, and Y. L. Chen, Magnetic Weyl semimetal phase in a Kagomé crystal, *Science* **365**, 1282 (2019).
- [8] N. Morali, R. Batabyal, P. K. Nag, E. Liu, Q. Xu, Y. Sun, B. Yan, C. Felser, N. Avraham, and H. Beidenkopf, Fermi-arc diversity on surface terminations of the magnetic Weyl semimetal $\text{Co}_3\text{Sn}_2\text{S}_2$, *Science* **365**, 1286 (2019).
- [9] Z. Liu, M. Li, Q. Wang, G. Wang, C. Wen, K. Jiang, X. Lu, S. Yan, Y. Huang, D. Shen, J.-X. Yin, Z. Wang, Z. Yin, H. Lei, and S. Wang, Orbital-selective Dirac fermions and extremely flat bands in frustrated kagome-lattice metal CoSn, *Nature Communications* **11**, 4002 (2020).
- [10] J.-X. Yin, W. Ma, T. A. Cochran, X. Xu, S. S. Zhang, H.-J. Tien, N. Shumiya, G. Cheng, K. Jiang, B. Lian, Z. Song, G. Chang, I. Belopolski, D. Multer, M. Litskevich, Z.-J. Cheng, X. P. Yang, B. Swidler, H. Zhou, H. Lin, T. Neupert, Z. Wang, N. Yao, T.-R. Chang, S. Jia, and M. Zahid Hasan, Quantum-limit Chern topological magnetism in TbMn_6Sn_6 , *Nature* **583**, 533 (2020).
- [11] B. R. Ortiz, S. M. L. Teicher, Y. Hu, J. L. Zuo, P. M. Sarte, E. C. Schueller, A. M. M. Abeykoon, M. J. Krogstad, S. Rosenkranz, R. Osborn, R. Seshadri, L. Balents, J. He, and S. D. Wilson, CsV_3Sb_5 : A \mathbb{Z}_2 Topological Kagome Metal with a Superconducting Ground State, *Phys. Rev. Lett.* **125**, 247002 (2020).
- [12] Z. Guguchia, C. Mielke, D. Das, R. Gupta, J. X. Yin,

- H. Liu, Q. Yin, M. H. Christensen, Z. Tu, C. Gong, N. Shumiya, M. S. Hossain, T. Gamsakhurdashvili, M. Elender, P. Dai, A. Amato, Y. Shi, H. C. Lei, R. M. Fernandes, M. Z. Hasan, H. Luetkens, and R. Khasanov, Tunable unconventional kagome superconductivity in charge ordered RbV_3Sb_5 and KV_3Sb_5 , *Nature communications* **14**, 153 (2023).
- [13] H. Zhao, H. Li, B. R. Ortiz, S. M. Teicher, T. Park, M. Ye, Z. Wang, L. Balents, S. D. Wilson, and I. Zeljkovic, Cascade of correlated electron states in the kagome superconductor CsV_3Sb_5 , *Nature* **599**, 216 (2021).
- [14] C. Mielke, D. Das, J.-X. Yin, H. Liu, R. Gupta, Y.-X. Jiang, M. Medarde, X. Wu, H. C. Lei, J. Chang, P. Dai, Q. Si, H. Miao, R. Thomale, T. Neupert, Y. Shi, R. Khasanov, M. Z. Hasan, H. Luetkens, and Z. Guguchia, Time-reversal symmetry-breaking charge order in a kagome superconductor, *Nature* **602**, 245 (2022).
- [15] L. Nie, K. Sun, W. Ma, D. Song, L. Zheng, Z. Liang, P. Wu, F. Yu, J. Li, M. Shan, D. Zhao, S. Li, B. Kang, Z. Wu, Y. Zhou, K. Liu, Z. Xiang, J. Ying, Z. Wang, T. Wu, and X. Chen, Charge-density-wave-driven electronic nematicity in a kagome superconductor, *Nature* **604**, 59 (2022).
- [16] H. Chen, H. Yang, B. Hu, Z. Zhao, J. Yuan, Y. Xing, G. Qian, Z. Huang, G. Li, Y. Ye, S. Ma, S. Ni, H. Zhang, Q. Yin, C. Gong, Z. Tu, H. Lei, H. Tan, S. Zhou, C. Shen, X. Dong, B. Yan, Z. Wang, and H.-J. Gao, Roton pair density wave in a strong-coupling kagome superconductor, *Nature* **599**, 222 (2021).
- [17] S.-Y. Yang, Y. Wang, B. R. Ortiz, D. Liu, J. Gayles, E. Derunova, R. Gonzalez-Hernandez, L. Šmejkal, Y. Chen, S. S. P. Parkin, S. D. Wilson, E. S. Toberer, T. McQueen, and M. N. Ali, Giant, unconventional anomalous Hall effect in the metallic frustrated magnet candidate, KV_3Sb_5 , *Science Advances* **6**, 10.1126/sciadv.abb6003 (2020).
- [18] X. Teng, L. Chen, F. Ye, E. Rosenberg, Z. Liu, J.-X. Yin, Y.-X. Jiang, J. S. Oh, M. Z. Hasan, K. J. Neubauer, B. Gao, Y. Xie, M. Hashimoto, D. Lu, C. Jozwiak, A. Bostwick, E. Rotenberg, R. J. Birgeneau, J.-H. Chu, M. Yi, and P. Dai, Discovery of charge density wave in a kagome lattice antiferromagnet, *Nature* **609**, 490 (2022).
- [19] X. Teng, J. S. Oh, H. Tan, L. Chen, J. Huang, B. Gao, J.-X. Yin, J.-H. Chu, M. Hashimoto, D. Lu, C. Jozwiak, A. Bostwick, E. Rotenberg, G. E. Granroth, B. Yan, R. J. Birgeneau, P. Dai, and M. Yi, Magnetism and charge density wave order in kagome FeGe , *Nature Physics* **19**, 814 (2023).
- [20] S. Shao, J.-X. Yin, I. Belopolski, J.-Y. You, T. Hou, H. Chen, Y. Jiang, M. S. Hossain, M. Yahyavi, C.-H. Hsu, Y. P. Feng, A. Bansil, M. Z. Hasan, and G. Chang, Intertwining of Magnetism and Charge Ordering in Kagome FeGe , *ACS Nano* **17**, 10164 (2023).
- [21] L. Wu, Y. Hu, D. Wang, and X. Wan, Novel three-dimensional Fermi surface and electron-correlation-induced charge density wave in FeGe , arXiv:2302.03622 (2023).
- [22] Y. Wang, Enhanced spin-polarization via partial G-dimerization as the driving force of the charge density wave in FeGe , *Physical Review Materials* **7**, 104006 (2023).
- [23] Z. Zhao, T. Li, P. Li, X. Wu, J. Yao, Z. Chen, S. Cui, Z. Sun, Y. Yang, Z. Jiang, Z. Liu, A. Louat, T. Kim, C. Cacho, A. Wang, Y. Wang, D. Shen, J. Jiang, and D. Feng, Photoemission Evidence of a Novel Charge Order in Kagome Metal FeGe , arXiv:2308.08336 (2023).
- [24] S. Wu, M. Klemm, J. Shah, E. T. Ritz, C. Duan, X. Teng, B. Gao, F. Ye, M. Matsuda, F. Li, X. Xu, M. Yi, T. Birol, P. Dai, and G. Blumberg, Symmetry breaking and ascending in the magnetic kagome metal FeGe , arXiv:2309.14314 (2023).
- [25] Z. Chen, X. Wu, S. Zhou, J. Zhang, R. Yin, Y. Li, M. Li, J. Gong, M. He, Y. Chai, X. Zhou, Y. Wang, A. Wang, Y.-J. Yan, and D.-L. Feng, Long-ranged charge order conspired by magnetism and lattice in an antiferromagnetic Kagome metal, arXiv:2307.07990 (2023).
- [26] C. Shi, Y. Liu, B. B. Maity, Q. Wang, S. R. Kotla, S. Ramakrishnan, C. Eisele, H. Agarwal, L. Noohinejad, Q. Tao, B. Kang, Z. Lou, X. Yang, Y. Qi, X. Lin, Z.-A. Xu, A. Thamizhavel, G.-H. Cao, S. van Smaalen, S. Cao, and J.-K. Bao, Disordered structure for long-range charge density wave order in annealed crystals of magnetic kagome FeGe , arXiv:2308.09034 (2023).
- [27] B. Zhang, J. Ji, C. Xu, and H. Xiang, Triple-Well Charge Density Wave Transition Driven by Partially Occupied Ge Electronic States in Kagome FeGe , arXiv:2307.10565 (2023).
- [28] J.-X. Yin, Y.-X. Jiang, X. Teng, M. S. Hossain, S. Mardanya, T.-R. Chang, Z. Ye, G. Xu, M. M. Denner, T. Neupert, B. Lienhard, H.-B. Deng, C. Setty, Q. Si, G. Chang, Z. Guguchia, B. Gao, N. Shumiya, Q. Zhang, T. A. Cochran, D. Multer, M. Yi, P. Dai, and M. Z. Hasan, Discovery of charge order and corresponding edge state in kagome magnet FeGe , *Phys. Rev. Lett.* **129**, 166401 (2022).
- [29] H. Miao, T. T. Zhang, H. X. Li, G. Fabbris, A. H. Said, R. Tartaglia, T. Yilmaz, E. Vescovo, J. X. Yin, S. Murakami, X. L. Feng, K. Jiang, X. L. Wu, A. F. Wang, S. Okamoto, Y. L. Wang, and H. N. Lee, Signature of spin-phonon coupling driven charge density wave in a kagome magnet, *Nature Communications* **14**, 6183 (2023).
- [30] Z. Chen, X. Wu, R. Yin, J. Zhang, S. Wang, Y. Li, M. Li, A. Wang, Y. Wang, Y.-j. Yan, and D.-l. Feng, Charge density wave with strong quantum phase fluctuations in Kagome magnet FeGe , arXiv:2302.04490 (2023).
- [31] H.-Y. Ma, J.-X. Yin, M. Z. Hasan, and J. Liu, Theory for charge density wave and orbital-flux state in antiferromagnetic kagome metal FeGe , arXiv:2303.02824 (2023).
- [32] H. Zhou, S. Yan, D. Fan, D. Wang, and X. Wan, Magnetic interactions and possible structural distortion in kagome FeGe from first-principles calculations and symmetry analysis, *Phys. Rev. B* **108**, 035138 (2023).
- [33] S. Cho, H. Ma, W. Xia, Y. Yang, Z. Liu, Z. Huang, Z. Jiang, X. Lu, J. Liu, Z. Liu, J. Li, J. Wang, Y. Liu, J. Jia, Y. Guo, J. Liu, and D. Shen, Emergence of New van Hove Singularities in the Charge Density Wave State of a Topological Kagome Metal RbV_3Sb_5 , *Phys. Rev. Lett.* **127**, 236401 (2021).
- [34] H. Tan, Y. Liu, Z. Wang, and B. Yan, Charge Density Waves and Electronic Properties of Superconducting Kagome Metals, *Phys. Rev. Lett.* **127**, 046401 (2021).
- [35] Y. Hu, X. Wu, B. R. Ortiz, S. Ju, X. Han, J. Ma, N. C. Plumb, M. Radovic, R. Thomale, S. D. Wilson, A. P. Schnyder, and M. Shi, Rich nature of Van Hove singularities in Kagome superconductor CsV_3Sb_5 , *Nature Com-*

- munications **13**, 2220 (2022).
- [36] Z. Liu, N. Zhao, Q. Yin, C. Gong, Z. Tu, M. Li, W. Song, Z. Liu, D. Shen, Y. Huang, K. Liu, H. Lei, and S. Wang, Charge-Density-Wave-Induced Bands Renormalization and Energy Gaps in a Kagome Superconductor RbV_3Sb_5 , *Phys. Rev. X* **11**, 041010 (2021).
- [37] M. Kang, S. Fang, J.-K. Kim, B. R. Ortiz, S. H. Ryu, J. Kim, J. Yoo, G. Sangiovanni, D. Di Sante, B.-G. Park, C. Jozwiak, A. Bostwick, E. Rotenberg, E. Kaxiras, S. D. Wilson, J.-H. Park, and R. Comin, Twofold van Hove singularity and origin of charge order in topological kagome superconductor CsV_3Sb_5 , *Nature Physics* **18**, 301 (2022).
- [38] X. Zhou, Y. Li, X. Fan, J. Hao, Y. Dai, Z. Wang, Y. Yao, and H.-H. Wen, Origin of charge density wave in the kagome metal CsV_3Sb_5 as revealed by optical spectroscopy, *Phys. Rev. B* **104**, L041101 (2021).
- [39] H. Luo, Q. Gao, H. Liu, Y. Gu, D. Wu, C. Yi, J. Jia, S. Wu, X. Luo, Y. Xu, L. Zhao, Q. Wang, H. Mao, G. Liu, Z. Zhu, Y. Shi, K. Jiang, J. Hu, Z. Xu, and X. J. Zhou, Electronic nature of charge density wave and electron-phonon coupling in kagome superconductor KV_3Sb_5 , *Nature Communications* **13**, 273 (2022).
- [40] Y. Xie, Y. Li, P. Bourges, A. Ivanov, Z. Ye, J.-X. Yin, M. Z. Hasan, A. Luo, Y. Yao, Z. Wang, G. Xu, and P. Dai, Electron-phonon coupling in the charge density wave state of CsV_3Sb_5 , *Phys. Rev. B* **105**, L140501 (2022).
- [41] G. Liu, X. Ma, K. He, Q. Li, H. Tan, Y. Liu, J. Xu, W. Tang, K. Watanabe, T. Taniguchi, L. Gao, Y. Dai, H.-H. Wen, B. Yan, and X. Xi, Observation of anomalous amplitude modes in the kagome metal CsV_3Sb_5 , *Nature Communications* **13**, 3461 (2022).
- [42] X. Zhou, Y. Li, X. Fan, J. Hao, Y. Xiang, Z. Liu, Y. Dai, Z. Wang, Y. Yao, and H. H. Wen, Electronic correlations and evolution of the charge density wave in the kagome metals AV_3Sb_5 ($A = \text{K}, \text{Rb}, \text{Cs}$), *Physical Review B* **107**, 165123 (2023).
- [43] M. M. Qazilbash, J. J. Hamlin, R. E. Baumbach, L. Zhang, D. J. Singh, M. B. Maple, and D. N. Basov, Electronic correlations in the iron pnictides, *Nature Physics* **5**, 647 (2009).
- [44] C. Setty, C. A. Lane, L. Chen, H. Hu, J.-X. Zhu, and Q. Si, Electron correlations and charge density wave in the topological kagome metal FeGe , arXiv:2203.01930 (2022).
- [45] X. Wu, X. Mi, L. Zhang, X. Zhou, M. He, Y. Chai, and A. Wang, Annealing tunable charge density wave order in a magnetic kagome material FeGe , arXiv:2308.01291 (2023).
- [46] M. Wenzel, E. Uykur, A. A. Tsirlin, S. Pal, R. M. Roy, C. Yi, C. Shekhar, C. Felser, A. V. Pronin, and M. Dressel, Intriguing low-temperature phase in the antiferromagnetic kagome metal FeGe , arXiv:2401.13474 (2024).